Cross-Beam Energy Transfer Saturation by Ion-Trapping–Induced Detuning

K. L. Nguyen,[1,2,3] L. Yin,[3] B. J. Albright,[3] A. M. Hansen,[1,2] D. H. Froula,[1] D. Turnbull,[1] R. K. Follett,[1] and J. P. Palastro[1]

[1]Laboratory for Laser Energetics, University of Rochester
[2]Department of Physics and Astronomy, University of Rochester
[3]Los Alamos National Laboratory

The performance of direct-drive inertial confinement fusion (ICF) implosions relies critically on the coupling of laser energy to the target plasma. Cross-beam energy transfer (CBET), the resonant exchange of energy between intersecting laser beams mediated by ponderomotively driven ion-acoustic waves (IAW's), inhibits this coupling by scattering light into unwanted directions. The variety of beam intersection angles and varying plasma conditions in an implosion results in IAW's with a range of phase velocities. Here, we show that CBET saturates through a resonance detuning that depends on the IAW phase velocity and that results from trapping-induced modifications to the ion distribution functions. For smaller phase velocities, the modifications to the distribution functions can rapidly thermalize in the presence of mid-*Z* ions, leading to a blue shift in the resonant frequency. For larger phase velocities, the modifications can persist, leading to a red shift in the resonant frequency. Ultimately, these results may reveal pathways toward CBET mitigation and inform reduced models for radiation-hydrodynamic codes to improve their predictive capability.

Laser-driven ICF experiments are subject to numerous nonlinear couplings between the electromagnetic waves and plasma waves. Among these couplings, CBET, the resonant exchange of energy between intersecting laser pulses mediated by ponderomotively driven IAW's, has emerged as particularly troublesome.[1] CBET inhibits the performance of both direct- and indirect-drive implosions by scattering light into unwanted directions.[2–4] In direct drive, this reduces the coupling of laser energy to the capsule, while in indirect drive, it can spoil the symmetry of the x-ray illumination. Both approaches have achieved some success in mitigating CBET by using independent wavelength shifts on the beams to detune the interaction.[5–8] More-extensive mitigation, however, requires pulses with a much larger bandwidth[9]—a technology in active development at LLE and the Naval Research Laboratory.[10–12]

Comprehensive, predictive models of CBET can guide both ongoing and future mitigation strategies and help define the expanded ICF design space that these strategies afford. Current integrated models of ICF implosions, using radiation-hydrodynamic simulations, typically implement simple linear models of CBET due to the computational expense associated with more-complete models. While more-sophisticated models have been developed,[13–16] common approximations include ray optics (i.e., speckle and diffractive effects are ignored) and a steady-state plasma response, while neglecting nonlinear processes.[17] This is in spite of a mounting body of work pointing to the importance of processes such as ion trapping, stochastic heating, two-ion decay, nonlinear sound waves, and IAW breakup.[18–23] Perhaps the most-convincing indication comes from a number of experiments that have observed nonlinear saturation.[24–26] The most recent of these experiments, performed on the OMEGA laser, demonstrated that, at high intensities, a drop in the power transferred from a pump to seed pulse was accompanied by an ~7× increase in the ion temperature.[26]

Motivated by this observation, this work provides a detailed description of the underlying physics responsible for CBET saturation for conditions relevant to these experiments. Specifically, we show that depending on the phase velocity of the IAW (v_p), CBET can saturate through two types of resonance detuning, both of which result from trapping-induced modifications to the ion distribution function. For "small" IAW phase velocities, the modifications to the distribution function rapidly thermalize in the presence of mid-*Z* ions, blue shifting the resonant IAW frequency. For "large" IAW phase velocities, the modifications to the

distribution function persist for a longer time and red shift the resonant frequency. These results, obtained using the collisional particle-in-cell code VPIC,[27] avoid many of the pitfalls associated with the reduced models used in radiation-hydrodynamic codes and provide insight into the evolution and feedback of CBET with the coronal plasma.

Figure 1 demonstrates that, in both the small and large v_p cases, CBET evolves through three stages: an initial linear stage (<5 ps), an early saturation stage (~5 to 20 ps), and a final late-time saturation stage (>20 ps). During each of these stages, the gain, i.e., $G = \ln(P^{out}/P^{in})$, where P^{in} and P^{out} are the probe input and output powers, tracks the electrostatic energy. The initial stage corresponds to transient growth of the IAW as the interaction attempts to evolve toward a linear, steady state.

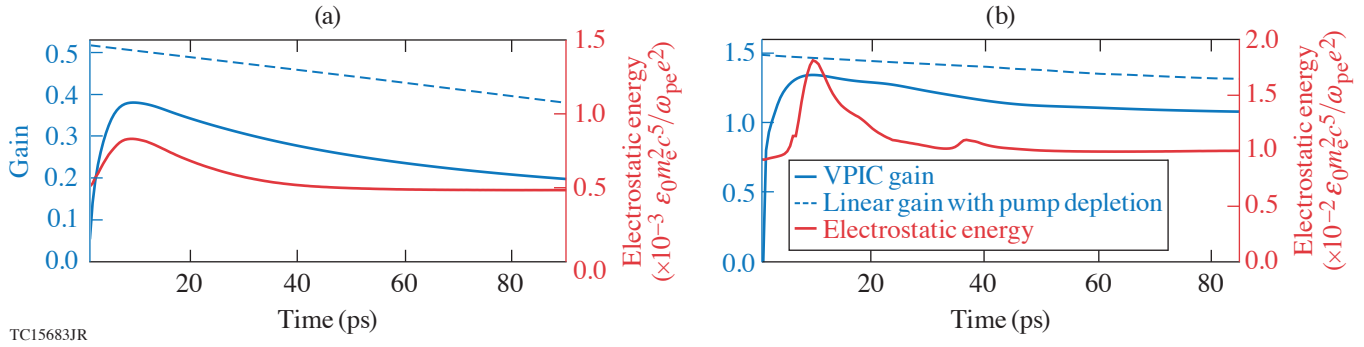

Figure 1
Evolution of the CBET gain and electrostatic energy for the (a) "small" and (b) "large" phase velocity cases. The CBET gain generally tracks the electrostatic energy. Due to an interplay of IAW transverse breakup and reduced Landau damping from ion trapping, the gain saturates at a value lower than the linear, steady-state gain.

Before this state can be reached, however, the interaction becomes nonlinear and the IAW undergoes transverse breakup.[28] The IAW initially exhibits coherent phase fronts, but after 20 ps, the fronts have broken up into smaller transverse structures. Due to its observed correlation with ion trapping, the breakup likely results from the trapped particle modulational instability (TPMI).[28–31] In the TPMI, the nonlinear frequency shift from ion trapping with inhomogeneity in the IAW amplitude creates variations in the phase velocity across the phase fronts. If a section of the phase front advances or retards by more than $\sim\pi/2$ with respect to adjacent sections, the front breaks. At this point, the wave amplitude crashes and the energy is transferred to the ions. The local dissipation of the wave prevents additional trapping and changes to the phase velocity. In fact, the rapid drop in electrostatic energy after ~10 ps results from initially trapped ions carrying away the energy of the now-broken IAW.

The rapid decay of the electrostatic energy (Fig. 1) is followed by a slow drop in the gain and marks the beginning of the late-time saturation stage. During this stage, the small and large v_p interactions exhibit strikingly different behaviors. Foremost, the gain drops substantially for small v_p and only modestly for large v_p. While both trends have their origin in ion-trapping–induced detuning, the cause of this detuning depends on the role of each ion species in collisional energy transfer and thermalization.

After ~50 ps, the plasma conditions and gain evolve slowly enough that CBET occurs in a quasi-steady state (Fig. 1). In this quasi-steady state, the kinetic coupling coefficient Im[Γ], calculated using the electron and ion distribution function and averaged over the interaction region, provides the response and resonant behavior of the plasma. For small v_p, the thermalization of the H and N ions causes a gradual blue shift in the resonant IAW frequency [Fig. 2(a)]. With the fixed wavelength shift of the probe beam, the gradual blue shift in resonant frequency causes the gain to drop. In addition, the increased damping from the modified distribution function has broadened the resonance peak and lowered its maximum. For large v_p all of the collision rates are generally lower than in the small-v_p case because of the larger phase velocity. This allows the trapping-induced modifications to the distribution function to persist for a much longer time. Consistent with the trapped ion frequency shift,[32,33] these modifications cause a red shift in the resonant frequency [Fig. 2(b)].

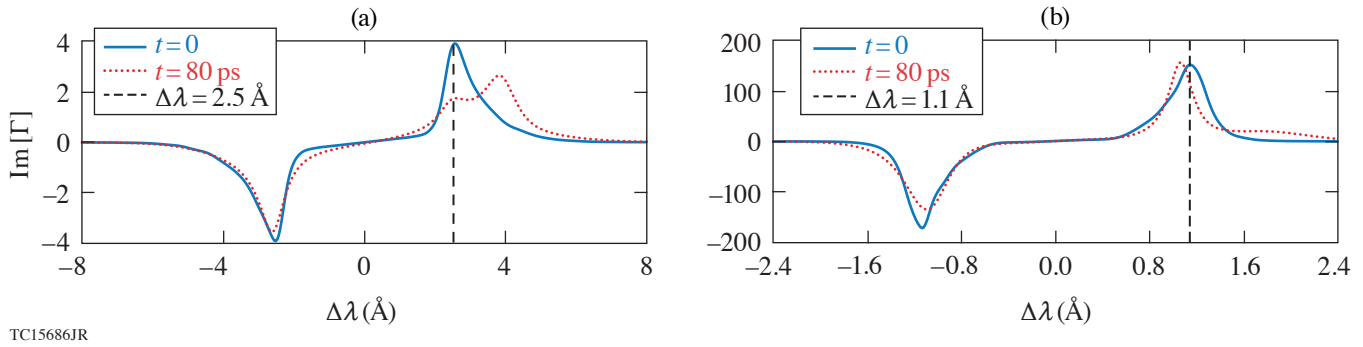

Figure 2
The Im[Γ], which determines the gain in the steady-state approximation, calculated using the electron- and ion-velocity distribution functions from VPIC at $t = 0$ and 80 ps. Initially, the IAW is driven on resonance for both the (a) small- (b) and large-v_p cases (intersection of the dashed black lines and the peak of the solid curve). Later, (a) the increase in ion temperatures and flow blueshift the peak in the small-v_p case, while (b) the persistent tails of the distribution function due to trapping redshift the peak in the large-v_p case. Both detunings cause the gain to drop.

This material is based upon work supported by the Department of Energy National Nuclear Security Administration under Award Number DE-NA0003856, the University of Rochester, and the New York State Energy Research and Development Authority. LANL work was performed under the auspices of the U.S. Department of Energy by the Triad National Security, LLC Los Alamos National Laboratory, and was supported by the LANL Directed Research and Development (LDRD) program and the LANL Office of Experimental Science Inertial Confinement Fusion program. VPIC simulations were run on the LANL Institutional Computing Clusters.

1. C. J. Randall, J. R. Albritton, and J. J. Thomson, Phys. Fluids **24**, 1474 (1981).
2. W. Seka *et al.*, Phys. Rev. Lett. **89**, 175002 (2002).
3. I. V. Igumenshchev *et al.*, Phys. Plasmas **17**, 122708 (2010).
4. A. L. Kritcher *et al.*, Phys. Rev. E **98**, 053206 (2018).
5. P. Michel *et al.*, Phys. Rev. Lett. **102**, 025004 (2009).
6. S. H. Glenzer *et al.*, Science **327**, 1228 (2010).
7. J. D. Moody *et al.*, Nat. Phys. **8**, 344 (2012).
8. J. A. Marozas *et al.*, Phys. Rev. Lett. **120**, 085001 (2018).
9. J. W. Bates *et al.*, Phys. Rev. E **97**, 061202(R) (2018).
10. C. Dorrer, J. Opt. Soc. Am. B **38**, 792 (2021).
11. J. Weaver *et al.*, Appl. Opt. **56**, 8618 (2017).
12. R. H. Lehmberg *et al.*, Phys. Rev. A **102**, 063530 (2020).
13. R. K. Follett *et al.*, Phys. Rev. E **98**, 043202 (2018).
14. A. Colaïtis *et al.*, Phys. Plasmas **26**, 032301 (2019).
15. A. Colaïtis *et al.*, Phys. Plasmas **26**, 072706 (2019)
16. A. Debayle *et al.*, Phys. Plasmas **26**, 092705 (2019).
17. A. Debayle *et al.*, Phys. Plasmas **25**, 052702 (2018).
18. E. A. Williams *et al.*, Phys. Plasmas **11**, 231 (2004).
19. P. Michel *et al.*, Phys. Rev. Lett. **109**, 195004 (2012).
20. P. Michel *et al.*, Phys. Plasmas **20**, 056308 (2013).
21. T. Chapman *et al.*, Phys. Rev. Lett. **119**, 055002 (2017).
22. S. Hüller *et al.*, Phys. Plasmas **27**, 022703 (2020).
23. L. Yin *et al.*, Phys. Plasmas **26**, 082708 (2019).
24. R. K. Kirkwood *et al.*, Phys. Rev. Lett. **89**, 215003 (2002).
25. D. Turnbull *et al.*, Plasma Phys. Control. Fusion **60**, 054017 (2018).

26. A. M. Hansen *et al.*, Phys. Rev. Lett. **126**, 075002 (2021).
27. K. J. Bowers *et al.*, Phys. Plasmas **15**, 055703 (2008).
28. L. Yin *et al.*, Phys. Rev. Lett. **99**, 265004 (2007).
29. W. L. Kruer, J. M. Dawson, and R. N. Sudan, Phys. Rev. Lett. **23**, 838 (1969).
30. R. L. Dewar, W. L. Kruer, and W. M. Manheimer, Phys. Rev. Lett. **28**, 215 (1972).
31. S. Brunner and E. J. Valeo, Phys. Rev. Lett. **93**, 145003 (2004).
32. G. J. Morales and T. M. O'Neil, Phys. Rev. Lett. **28**, 417 (1972); 709(E) (1972).
33. R. L. Berger *et al.*, Phys. Plasmas **20**, 032107 (2013).